THE JOURNAL OF BIOLOGICAL CHEMISTRY
© 1990 by The American Society for Biochemistry and Molecular Biology, Inc.

Vol. 265, No. 4, Issue of February 5, pp. 2399-2408, 1990
Printed in U.S.A.

Toxic Injury from Mercuric Chloride in Rat Hepatocytes*

(Received for publication, August 3, 1989)

Anna-Liisa Nieminen, Gregory J. Gores‡, Thomas L. Dawson, Brian Herman, and John J. Lemasters§

From the Laboratories for Cell Biology, Department of Cell Biology & Anatomy, School of Medicine, University of North Carolina, Chapel Hill, North Carolina 27599-7090

The relationship between cytosolic free Ca^{2+}, mitochondrial membrane potential, ATP depletion, pyridine nucleotide fluorescence, cell surface blebbing, and cell death was evaluated in rat hepatocytes exposed to $HgCl_2$. In cell suspensions, 50 μM $HgCl_2$ oxidized pyridine nucleotides between ½ and 2 min, caused ATP depletion between 2 and 5 min, and produced an 89% loss of cell viability after 20 min. Rates of cell killing were identical in high (1.2 mM) and low (2.6 μM) Ca^{2+} buffers. Cytosolic free Ca^{2+} was determined in 1-day cultured hepatocytes by ratio imaging of Fura-2 employing multiparameter digitized video microscopy. In high Ca^{2+} medium, $HgCl_2$ caused a 3–4-fold increase of free Ca^{2+} beginning after 6–7 min, but free Ca^{2+} did not change in low Ca^{2+} medium. Bleb formation occurred after about 4–5 min in both buffers prior to any increase of free Ca^{2+}. Subsequently, in high Ca^{2+} medium, blebs became hot spots of free Ca^{2+} (>600 nM). After about 2 min of exposure to $HgCl_2$, rhodamine 123 fluorescence redistributed from mitochondrial to cytosolic compartments signifying collapse of the mitochondrial membrane potential. The results taken together demonstrate that bleb formation, ATP depletion, and the onset of cell death are not dependent on an increase of cytosolic free Ca^{2+}. $HgCl_2$ toxicity appears to be a consequence of inhibition of oxidative phosphorylation leading to ATP depletion and cell death.

The role of calcium in cell injury has been under intensive investigation in recent years. Work from several laboratories has led to the working hypothesis that anoxic and toxic injury causes cytosolic free calcium to increase which in turn initiates a sequence of events leading to irreversible injury and cell killing (1, 2). As a consequence of increased free Ca^{2+}, it is hypothesized that alterations of the cytoskeleton lead to cell surface bleb formation and subsequent rupture, that hydrolases (*e.g.* proteases, phospholipases, and endonucleases; Refs. 2–4) are activated further promoting lethal cell injury, and that Ca^{2+} enters mitochondria resulting in uncoupling and ATP depletion.

Our recent work, however, has failed to support the calcium hypothesis of cell killing. Using inhibitors of glycolysis and oxidative phosphorylation to mimic ATP depletion of anoxia (chemical hypoxia), we observed that an increase of cytosolic free calcium did not precede cell surface blebbing or the onset of cell death (5, 6). Nonetheless, increases of cell calcium may be important in other forms of cell injury. Our goal, therefore, has been to identify toxic chemicals which produce increases of cytosolic free Ca^{2+} so that the injurious effects, if any, of increased cytosolic free calcium may be characterized.

$HgCl_2$ is a potent nephrotoxin which is directly cytotoxic (7, 8). Recently, Smith *et al.* (9) reported an increase of free calcium in suspensions of rabbit kidney proximal tubule cells following exposure to $HgCl_2$. This finding was interpreted to support the hypothesis that Ca^{2+} influxes induced by toxic chemicals initiate lethal cell injury. A second action of $HgCl_2$ is depolarization, uncoupling, and respiratory inhibition of mitochondria, effects which might also account for lethal cell injury (10, 11). The objective of this investigation, therefore, was to compare the effects of $HgCl_2$ on cytosolic free calcium and mitochondrial membrane potential in single living cells. The results show that cytosolic free Ca^{2+} does increase following exposure to $HgCl_2$ in Ca^{2+}-containing medium but that this rise of free calcium does not accelerate cell killing. Rather, $HgCl_2$ appears to target mitochondria for its toxic effects.

EXPERIMENTAL PROCEDURES

Hepatocyte Isolation—Hepatocytes were isolated by collagenase perfusion of livers from overnight fasted male Sprague-Dawley rats (200–250 g) as described previously (12). For viability assays, freshly isolated hepatocytes were suspended in Krebs-Henseleit-Hepes[1] buffer (KHB) containing 2 mg/ml BSA or washed twice (50 *g*-min) in Ca^{2+}-free KHB containing BSA and resuspended in the same buffer. For cell culture, hepatocytes were diluted to 500,000 cells/ml in Waymouth's medium MB-752/1 containing 2 mM L-glutamine, 27 mM $NaHCO_3$, 5% fetal calf serum, 100 nM insulin, and 10 nM dexamethasone. Aliquots of 1 ml were cultured on 22-mm square glass coverslips coated with rat tail collagen (13) in 35 × 10-mm Petri dishes to produce subconfluent cultures for single cell analysis. Hepatocytes were used after 20–36 h of culture in humidified 5% CO_2, 95% air at 37 °C.

* This work was supported in part by Grants AG07218 and DK30874 from the National Institutes of Health and Grant N-00014 from the Office of Naval Research. A preliminary report of portions of this work was presented at the 72nd Annual Meeting of the Federation of American Societies for Experimental Biology, Las Vegas, Nevada, May 1–5, 1988 (52). The costs of publication of this article were defrayed in part by the payment of page charges. This article must therefore be hereby marked "*advertisement*" in accordance with 18 U.S.C. Section 1734 solely to indicate this fact.

‡ Recipient of an Individual Research Service Award from the National Institutes of Health and a Mayo Foundation Scholar. Present address: GI Research Unit, Mayo Clinic, Rochester, MN 55905.

§ To whom correspondence should be addressed: Laboratories for Cell Biology, Dept. of Cell Biology & Anatomy, School of Medicine, University of North Carolina, Campus Box 7090, 236 Swing Bldg., Chapel Hill, NC 27599-7090.

[1] The abbreviations used are: Hepes, *N*-2-hydroxyethylpiperazine-*N'*-2-ethanesulfonic acid; KHB, Krebs-Henseleit-Hepes buffer containing 118 mM NaCl, 24.9 mM $NaHCO_3$, 1.27 mM $CaCl_2$, 1.19 mM KH_2PO_4, 1.18 mM $MgSO_4$, 4.74 mM KCl, and 25 mM NaHepes buffer, pH 7.4; KRH, Krebs-Ringers-Hepes buffer containing 115 mM NaCl, 5 mM KCl, 2 mM $CaCl_2$, 1 mM KH_2PO_4, 1.2 mM $MgSO_4$, 25 mM NaHepes buffer, pH 7.4; BSA, bovine serum albumin, fraction V; Fura-2-AM, acetoxymethyl ester of Fura-2; MDVM, multiparameter digitized video microscopy; EGTA, [ethylenebis(oxyethylenenitrilo)] tetraacetic acid; MOPS, 4-morpholinepropanesulfonic acid; *g*-min, gravity minutes.

Cell Viability Assay—Propidium iodide labels the nuclei of nonviable cells with an enhancement of fluorescence. Cell viability assays were performed by incubating freshly isolated hepatocytes (100,000 cells/ml) with 1 μM propidium iodide (14). Fluorescence was monitored with a Sequoia-Turner Model 450 filter fluorometer (Mountain View, CA) using 520-nm (8-nm band pass) excitation and 605-nm (long pass) emission filters. After measuring basal fluorescence (A), 0–100 μM $HgCl_2$ was added, and fluorescence was measured every 5 min for 30 min. Individual experiments were terminated by adding 375 μM digitonin to permeabilize all cells, and a final fluorescence measurement (B) was obtained 20 min later. Percent cell viability at time points during the incubation was calculated by the formula

$$V = 100 \times (B - X)/(B - A)$$

where V is viability in percent and X is fluorescence at any given time. After 30 min of exposure to $HgCl_2$, cell viability was 86, 80, 22, 8, and 1%, respectively, after 0, 10, 20, 50, and 100 μM $HgCl_2$. Since 50 μM was a concentration used in a previous study of $HgCl_2$ cytotoxicity (9, 15) and since 50 μM produced close to the maximum rate of cell killing, this concentration of $HgCl_2$ was employed in our subsequent experiments.

Concentration of Extracellular Free Ca^{2+} of Hepatocyte Suspensions in Low Ca^{2+} Medium—To determine extracellular free Ca^{2+} for hepatocytes resuspended in Ca^{2+}-free KRH (low Ca^{2+} medium), hepatocytes (6×10^6/ml) were washed twice with Ca^{2+}-free KRH and resuspended in the same buffer to 100,000 cells/ml. The cell suspension was again centrifuged, and Fura-2 free acid (1 μM) was added to the supernatant. Fluorescence was measured at an excitation wavelength of 340 nm (2-nm slit) and an emission wavelength of 510 nm (10-nm slit) with a Perkin-Elmer Model 850-40 fluorescence spectrophotometer (Norwalk, CT). EGTA (1 mM) and $CaCl_2$ (2 mM) were added subsequently to determine Ca^{2+}-independent and Ca^{2+}-dependent fluorescence. Assuming a K_d of 168 nM, the concentration of Ca^{2+} in the cell free supernatant was 2.6 μM. In parallel experiments, free Ca^{2+} in low Ca^{2+} medium prior to addition of cells was determined to be 1.6 μM.

Measurement of ATP—Freshly isolated hepatocytes (100,000/ml) were incubated at 37 °C in low or high Ca^{2+} KRH buffer containing 2 mg/ml BSA. Aliquots (3 ml) were quenched with 240 μl of 11.7 M $HClO_4$, vortexed, and cooled on ice. After centrifugation (4000 × g-min) in a tabletop centrifuge, the supernatants were neutralized with 5 M KOH and 0.4 M imidazole, centrifuged again, and passed through 0.45-μm Gelman Acrodisc filters (Ann Arbor, MI). ATP was determined by reverse-phase high performance liquid chromatography modified from Schweinsberg and Loo (16) and Jones (17). The chromatography system consisted of a Series 10 pump module, Model LC-95 UV-visible spectrophotometric detector operating at 260 nm and Model LCI 100 laboratory computer integrator (Perkin-Elmer, Norwalk, CT), and a Model 2360 gradient programmer (ISCO, Lincoln, NB). Flow rate was 1 ml/min through a 25-cm Whatman PartiSphere C_{18} (5 μm) reverse-phase column (American Scientific Products, McGaw Park, IL). Mobile phases were 100 mM KP_i buffer, pH 6.0 (buffer A) and 100 mM KP_i buffer, 5% methanol, pH 6.0 (buffer B). The gradient program was: 100% buffer A, 8.5 min; gradient to 80% buffer A and 20% buffer B, 0.5 min; 80% buffer A and 20% buffer B, 6 min; gradient to 100% buffer B, 0.5 min, 100% buffer B, 10 min, and 100% buffer A, 10 min. ATP eluted after about 6 min. ATP standards were assayed by their absorbance at 259 nm.

Concentration of Fura-2 in Loaded Hepatocytes—Freshly isolated hepatocytes (2×10^6/ml) were loaded with 3.5 μM Fura-2-AM in KRH buffer for 30 min at 37 °C, washed twice in Ca^{2+}-free KRH, and resuspended in Ca^{2+}-free KRH, pH 7.4. After permeabilization with 100 μM digitonin or 0.1% Triton X-100 and centrifugation (1000 × g-min), fluorescence of the supernatants was measured with the fluorescence spectrophotometer at excitation wavelengths of 340, 365, and 380 nm (2-nm slit) and an emission wavelength of 510 nm (10-nm slit). EGTA (1 mM) and $CaCl_2$ (2 mM) were added sequentially to determine Ca^{2+}-independent and Ca^{2+}-dependent fluorescence. Standard curves were obtained with known amounts of Fura-2 free acid.

Effect of $HgCl_2$ on the Dissociation Constant of Fura-2—Fluorescence of Fura-2 (1 μM) in Ca^{2+}-EGTA buffers was measured in the presence and absence of 50 μM $HgCl_2$. Dissociation constants (K_d) were determined by Scatchard analysis (18).

Multiparameter Digitized Video Microscopy (MDVM)—Fluorescence measurements in single cultured hepatocytes were performed using an MDVM system essentially as described previously (19). Briefly, the microscope was a Zeiss IM-35 inverted fluorescence microscope (Thornwood, NY) equipped with phase contrast optics. Excitation light was provided by a 100-watt mercury vapor lamp or xenon lamp and passed through an interference and neutral density filter wheel assembly to select wavelength and intensity under computer control. A shutter, also under computer control, automatically blocked the excitation light source between measurements. A low light-intensified, silicon-intensified target (ISIT) video camera (Model 66, MTI-Dage, Michigan City, IN) collected fluorescent images which were digitized with a QVG/AFA-123 video acquisition and display board set (Imaging Technologies, Woburn, MA) operating in a MicroPDP 11/23 computer (Digital Equipment Corporation, Maynard, MA) for frame-averaging, background subtraction, ratioing, and storage on 8-inch floppy disks. Experiments were also routinely recorded with a half-inch time-lapse video casette recorder (Model TC3900, RCA, Lancaster, PA).

For calcium measurements, cultured hepatocytes were loaded with 3.5 μM Fura-2-AM for 30 min at 37 °C in culture medium. Cells were washed three times with KHB and mounted on the microscope. Temperature was maintained at 37 °C using an air curtain incubator (Laboratory Products, Inc., Boston, MA). Cells were excited at Ca^{2+}-sensitive and Ca^{2+}-insensitive wavelengths of 340 and 365 nm, respectively. Fluorescence was imaged through a 395-nm dichroic reflector and 420-nm-long pass filter. Typically, 64 video frames were averaged to obtain a single image (2.1-s acquisition time). Background images were obtained in adjacent empty areas of the coverslip to correct for instrumental noise. After background subtraction, the image at 340 nm was divided by the image of 365 nm on a pixel-by-pixel basis. The mean values of pixel ratios for individual cells were compared with values obtained with the same settings using Fura-2-containing Ca^{2+}-EGTA buffers (20). In separate experiments, autofluorescence was measured in cells which had not been loaded with Fura-2. Fluorescence of nonloaded cells was less than 10% of that of Fura-2-loaded cells. No attempt was made to correct for this small level of autofluorescence.

To monitor mitochondrial membrane potential, cultured hepatocytes were loaded with 800 nM rhodamine 123 (5, 21, 22) using the same loading conditions as for Fura-2-AM. Cells were subsequently mounted on the microscope and incubated in KHB containing propidium iodide (1 μM), a fluorescent probe which labels the nuclei of nonviable cells (23). Fluorescence of rhodamine 123 was imaged using a 450–490-nm excitation filter, a 510-nm dichroic reflector, and a 530-nm long pass filter. Fluorescence of propidium iodide was imaged using a 554-nm excitation filter, a 580-nm dichroic reflector, and a 580-nm long pass filter.

For localization of Fura-2 in cultured hepatocytes, cells were co-loaded with rhodamine 123 as described above and incubated in Ca^{2+}-free KRH supplemented with 5 mM succinate. Digitonin at increasing concentrations (20 and 100 μM) and 0.1% Triton were then added to release Fura-2 sequentially from cytosolic, lysosomal, and mitochondrial compartments. The Ca^{2+}-free, succinate-containing medium prevented mitochondrial depolarization after digitonin.

To label lysosomes, rats were injected with rhodamine-dextran (20 mg/100 g body weight, intraperitoneal) 16 h prior to isolation of hepatocytes (24). Fluorescence of rhodamine-dextran was imaged at the same wavelengths as propidium iodide.

Pyridine Nucleotide Fluorescence—Freshly isolated hepatocytes (100,000 cells/ml) were resuspended in KRH buffer, and fluorescence of reduced pyridine nucleotides was recorded continuously using the fluorescence spectrophotometer. Cells were excited at 340 nm (2-nm slit) and emission was collected at 450 nm (10-nm slit).

Materials—Fura-2 and Fura-2-AM were purchased from Molecular Probes (Eugene, OR); rhodamine 123 was from Eastman Kodak Co.; propidium iodide, rhodamine-dextran (72.2 kDa average molecular weight), BSA fraction V, digitonin, mercuric chloride, imidazole, and probenecid were from Sigma; Hepes was from Boehringer Mannheim; Waymouth's medium MB252/1 was from Gibco Laboratories; Type II collagenase was from Cooper Biomedical (Malvern, PA); insulin was from Squibb-Novo, Inc. (Princeton, NJ); dexamethasone sodium phosphate was from LyphoMed, Inc. (Rosemont, IL); Br-A23187 was from Calbiochem. Other reagents were of analytical grade obtained from the usual commercial sources.

RESULTS

Intracellular Concentration of Fura-2 in Loaded Hepatocytes—Suspensions of isolated hepatocytes were incubated for 30 min with 3.5 μM Fura-2-AM as described under "Experi-

mental Procedures." The cells were washed in Ca^{2+}-free KRH and digitonin (100 μM) or Triton X-100 (0.1%) was added. Fura-2 release was slightly greater with Triton X-100 than with digitonin, indicating that a small proportion of Fura-2 (7%) was in a digitonin inaccessible compartment such as mitochondria. Assuming that the Fura-2 released by 100 μM digitonin was in an extramitochondrial cell volume of 4.6 μl/10^6 cells (25, 26), intracellular Fura-2 concentration was 52 μM. (Table I).

Fluorescence Spectra of Fura-2 Released from Loaded Hepatocytes—Fluorescence was measured in supernatants of Fura-2 loaded cells after digitonin treatment. 340/365-nm ratios in EGTA- and Ca^{2+}-saturated buffers were nearly identical to those for Fura-2 free acid (Table II). However, 340/380-nm ratios in Ca^{2+}-saturated buffer averaged almost 50% less than for Fura-2 free acid, suggesting the presence of incomplete hydrolysis products of Fura-2 AM which Scanlon *et al.* (27) have shown to have excitation maxima at 390–400 nm. For this reason, we employed 340/365-nm ratios to generate standard curves for measuring cytosolic free Ca^{2+} in single cultured cells. Moreover, 365 nm is near the isoemissive point for Fura-2 and could be employed to monitor Fura-2 leakage from cells after exposure to toxic chemicals.

The K_d of Fura-2 for Ca^{2+} was determined from measurements of fluorescence in EGTA buffers of varying Ca^{2+} concentrations as described under "Experimental Procedures." For 1 μM Fura-2 free acid, we observed a K_d of 168 nM (Table II). In the presence of 50 μM $HgCl_2$, the K_d was 165 nM. Therefore, $HgCl_2$ at concentrations used in this study did not affect the affinity of Fura-2 for Ca^{2+}. Similarly, $HgCl_2$ did not change the absolute fluorescence of Fura-2 (data not shown).

Subcellular Localization of Fura-2 in Single Cultured Hepatocytes—To localize Fura-2 within living cells, intracellular compartments were sequentially opened by increasing concentrations of digitonin. Digitonin at low concentrations causes selective permeabilization of the plasma membrane with sparing of intracellular organelles. At higher concentrations, cholesterol-containing organelles are permeabilized with sparing of low-cholesterol mitochondria (28, 29). In order to document these selective effects of digitonin, we co-loaded additional fluorescent probes with specificity for mitochondria (rhodamine 123; Fig. 1*C*) or lysosomes (rhodamine-dextran; Fig. 2*B*) before exposing the cells to digitonin. A Ca^{2+}-

TABLE I

Fura-2 release by digitonin and Triton X-100 from freshly isolated and cultured hepatocytes

Freshly isolated hepatocytes and 1-day cultured hepatocytes were loaded with Fura-2 AM as described under "Experimental Procedures." After detergent treatment, Fura-2 was quantitated in supernatants of cell suspensions using a spectrofluorometer and in single cultured cells using MDVM. In cell suspensions, 100 μM digitonin released 0.24 ± 0.05 nmol of Fura-2/10^6 cells (n = 4). Assuming a cellular volume of 5.8 μl/10^6 cells (25) and that 80% of cellular volume is nonmitochondrial (26), intracellular Fura-2 concentration was 52 ± 11 μM (n = 4). Data represent means ± S.E. ($n \geq 3$).

Treatment	Fura-2 in supernatant (spectrofluorometer)[a]	Remaining Fura-2 in cells (MDVM)[b]
20 μM digitonin	ND[c]	16.7 ± 4.7%
100 μM digitonin	93.1 ± 3.2%	6.0 ± 2.5%
0.1% Triton X-100	100%	Below detection (<1%)

[a] Calculated as percent of Fura-2 fluorescence released by Triton X-100.
[b] Calculated as percent of Fura-2 fluorescence prior to detergents.
[c] Not determined.

TABLE II

Ratio values at 340/365 and 340/380 nm for fluorescence released from Fura-2 loaded hepatocytes

Freshly isolated hepatocytes were loaded with Fura-2-AM and washed in Ca^{2+}-free KRH as described under "Experimental Procedures." After treatment with 100 μM digitonin, fluorescence ratio values at 340/365 and 340/380 nm were determined in cell free supernatants after sequential additions of EGTA (1 mM) and Ca^{2+} (2 mM). Ratio values for Fura-2 free acid were determined under identical conditions. Dissociation constants of Fura-2 for Ca^{2+} ion were determined from Scatchard plots of fluorescence (340-nm excitation, 510-nm emission) of Fura-2 (1 μM) in Ca^{2+}-EGTA buffers (10 mM EGTA, 100 mM KCl, 10 mM K-MOPS, pH 7.2, pCa 5.9–7.2, 23 °C) in the presence and absence of 50 μM $HgCl_2$. Data represent means ± S.E. (n = 2).

Treatment	Fluorescence ratios		
	340/365	340/380	K_d
			nM
Supernatant of digitonin-treated hepatocytes			ND[a]
1 mM EGTA	0.81 ± 0.002	1.05 ± 0.006	
2 mM $CaCl_2$	4.20 ± 0.022	25.3 ± 1.80	
Fura-2 free acid			168
1 mM EGTA	0.83 ± 0.020	1.10 ± 0.038	
2 mM $CaCl_2$	4.64 ± 0.167	53.5 ± 2.89[b]	
Fura-2 free acid + 50 μM $HgCl_2$			165

[a] Not determined.
[b] $p < 0.02$ compared to supernatant by two-tailed analysis of variance.

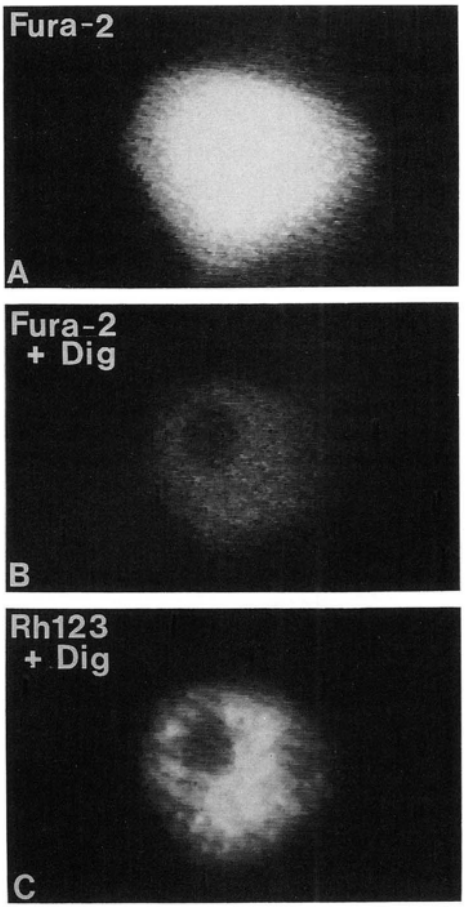

FIG. 1. **Subcellular localization of Fura-2 by MDVM: mitochondria.** A cultured hepatocyte was loaded with Fura-2-AM and rhodamine 123 as described under "Experimental Procedures" and incubated in Ca^{2+}-free KRH containing 5 mM succinate. Fura-2 fluorescence excited at 365 nm was diffuse (*A*). After addition of 100 μM digitonin, most Fura-2 fluorescence disappeared (*B*), but rhodamine 123 fluorescence of mitochondria remained intact (*C*).

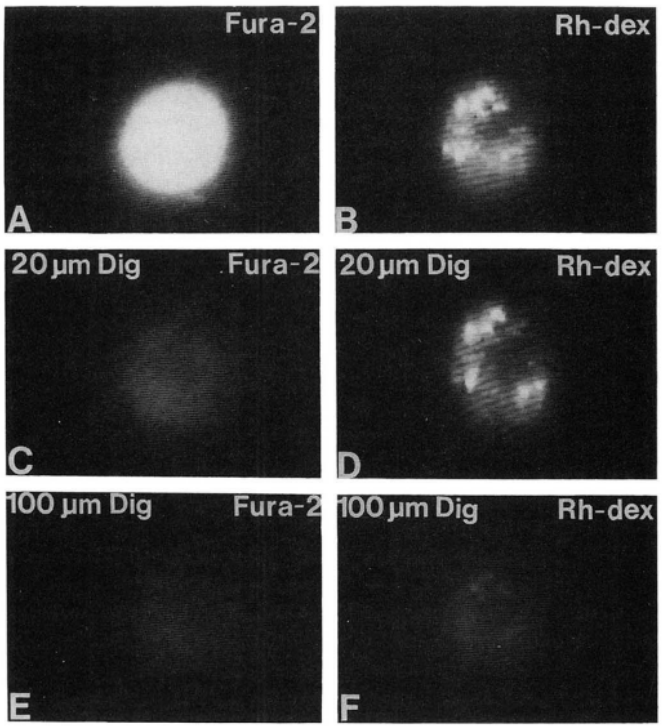

FIG. 2. **Subcellular localization of Fura-2 by MDVM: lysosomes.** A cultured hepatocyte was co-loaded with rhodamine-dextran and Fura-2 as described under "Experimental Procedures" and incubated in KRH. Fura-2 fluorescence excited at 365 nm was diffuse (*A*), whereas fluorescence of rhodamine-dextran in lysosomes was punctate (*B*). After 20 μM digitonin, most Fura-2 fluorescence was lost (*C*), but rhodamine-dextran fluorescence remained punctate and bright (*D*). After 100 μM digitonin, rhodamine-dextran fluorescence was lost virtually entirely (*F*). A slight additional loss of Fura-2 fluorescence also occurred which cannot be appreciated in the photographic print (*E*) (see Table I).

free, succinate-containing KRH buffer was employed to prevent mitochondrial swelling and depolarization after plasma membrane permeabilization. Preliminary experiments established that 20 and 100 μM digitonin were specific for permeabilizing the plasma membrane and nonmitochondrial organelles, respectively. After addition of the detergents, total fluorescence of Fura-2 inside single cells was measured (Table I), and Figs. 1 and 2 show representative experiments demonstrating qualitative changes in the actual fluorescence images. After 20 μM digitonin, 83% of Fura-2 fluorescence at the Ca^{2+}-insensitive wavelength of 365 nm was released (Table I, Fig. 2*C*), but rhodamine 123 fluorescence and rhodamine-dextran fluorescence (Fig. 2*D*) were unchanged. After 100 μM digitonin, a small additional release (11%) of Fura-2 fluorescence occurred (Table I, Fig. 2*E*) and rhodamine-dextran fluorescence disappeared. Punctate mitochondrial labeling with rhodamine 123 remained after 100 μM digitonin (Fig. 1*C*), but after 0.1% Triton X-100, rhodamine 123 fluorescence was no longer detectable (data not shown). In good agreement with Fura-2 release from cell suspensions, these results indicated that 83% of Fura-2 was localized to cytosol, 11% to lysosomes and other endomembrane compartments (endosomes, endoplasmic reticulum, etc.) and 6% to mitochondria. On the basis of the predominantly cytosolic localization of Fura-2, we employed ratio-imaging of Fura-2 fluorescence to measure cytosolic free Ca^{2+} in single cultured hepatocytes with no attempt to correct measured fluorescence ratios for noncytosolic loading of Fura-2.

Effect of $HgCl_2$ on Cytosolic Free Ca^{2+}—Cytosolic free Ca^{2+} was measured in individual cultured hepatocytes after exposure to 50 μM $HgCl_2$ (Fig. 3). In high Ca^{2+} medium, a 3–4-fold increase of free Ca^{2+} occurred beginning after 6–7 min of exposure. Under these conditions, cells lost viability after 15–20 min as indicated by nuclear staining with propidium iodide (data not shown). In low Ca^{2+} medium, cytosolic free calcium did not increase after 50 μM $HgCl_2$, although individual cells again lost viability after 15 to 20 min. Bleb formation observed by phase contrast optics occurred within 4–5 min of $HgCl_2$ addition in both high and low Ca^{2+} medium. Notably, bleb formation occurred prior to any change of free Ca^{2+}. In Fig. 3, cytosolic free Ca^{2+} was measured at 2.5-min intervals. Since previous work by Smith and co-workers (9) suggested an early transient rise of Ca^{2+} after $HgCl_2$, we also measured Ca^{2+} at 20-s intervals but observed no transient changes (Fig. 4*A*).

To observe possible interference by $HgCl_2$ on Fura-2 fluorescence *in situ*, Fura-2-loaded cultured hepatocytes were treated with Br-A23187, a nonfluorescent Ca^{2+} ionophore. In control cells, 50 μM Br-A23187 produced an immediate increase of cytosolic free Ca^{2+} to a new steady state level of about 325 nM (Fig. 4*B*). A similar increase occurred when Br-A23187 was added 1 min after the addition of 50 μM $HgCl_2$ (Fig. 4*A*). Since in the absence of Br-A23187, Ca^{2+} did not increase until after 6–7 min of exposure to $HgCl_2$ (Figs. 3 and 4*A*), these findings demonstrate directly that fluorescence of Fura-2-loaded cells remains responsive to changes of free Ca^{2+} after exposure to $HgCl_2$.

Spatial Distribution of Cytosolic Free Calcium—The spatial distribution of free Ca^{2+} within single cells was represented as pseudocolor maps. In a representative experiment in high Ca^{2+} medium, basal free Ca^{2+} averaged 175 nM and was evenly distributed (Fig. 5*A*). After 6 min of exposure to $HgCl_2$, cell surface blebs had formed as assessed by bright field phase contrast microscopy and also seen in the pseudo-color image, but average free Ca^{2+} was 160 nM and still homogeneous throughout the cell (Fig. 5*B*). After 16 min, free Ca^{2+} distribution was inhomogenous, and highest concentrations exceeding 600 nM were observed inside the blebs (Fig. 5*C*).

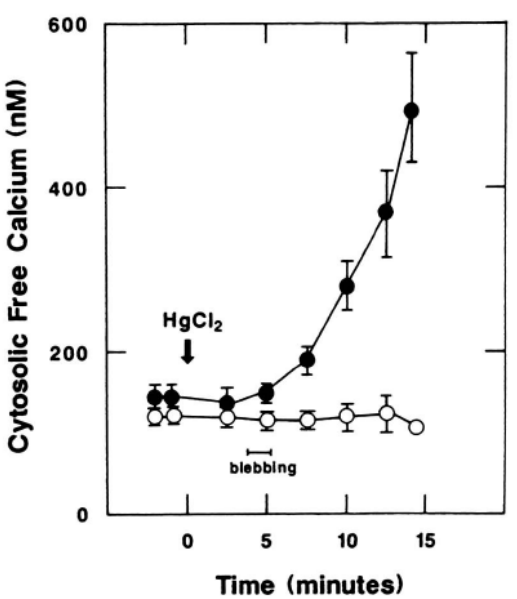

FIG. 3. **Cytosolic free Ca^{2+} of cultured hepatocytes after $HgCl_2$ in low and high Ca^{2+} media.** Cultured hepatocytes were incubated in KHB buffer containing 1.27 mM $CaCl_2$ (high Ca^{2+}, ●) or no added Ca^{2+} (low Ca^{2+}, ○). $HgCl_2$ (50 μM) was added where indicated. Cytosolic free Ca^{2+} was measured by ratio imaging of Fura-2 fluorescence using MDVM as described under "Experimental Procedures." Data represents means ± S.E. ($n \geq 5$).

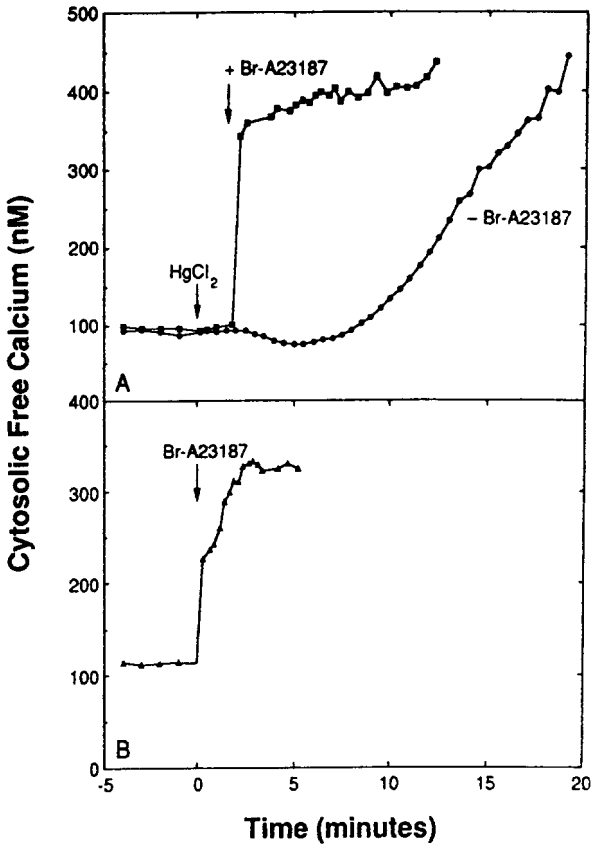

FIG. 4. **Effect of $HgCl_2$ on the response of Fura-2-loaded hepatocytes to Br-A23187.** Fura-2-loaded cultured hepatocytes were incubated in KRH buffer. $HgCl_2$ (50 μM) in the absence (A, ●) and presence of Br-A23187 (50 μM) (*A*, ■) and Br-A23187 alone (*B*) were added where indicated (*arrows*). Cytosolic free Ca^{2+} was measured by ratio imaging of Fura-2 fluorescence using MDVM as described under "Experimental Procedures." One experiment representative of two.

Subsequently, Fura-2 leaked to the extent that fluorescent images could no longer be obtained.

In a representative experiment in low Ca^{2+} medium, free Ca^{2+} averaged 115 nM, slightly lower than in high Ca^{2+} medium (Fig. 5*D*). After 7 min of exposure to $HgCl_2$, blebbing was apparent, but free Ca^{2+} concentration had not increased (Fig. 5*E*). After 16 min, free Ca^{2+} still had not increased (Fig. 5*F*), despite the presence of large, well developed blebs. After longer than 16 min, Fura-2 again leaked entirely from the cell.

Fura-2 Leakage after Exposure to $HgCl_2$—Absolute fluorescence at 340 and 365 nm was also monitored in order to follow Fura-2 leakage from the cells (Fig. 6). Before addition of $HgCl_2$, fluorescence at both wavelengths remained constant for more than 30 min without evidence of photobleaching or dye leakage from the cells (data not shown). Shortly after $HgCl_2$, however, a 40–50% increase of both 340 and 365 nm fluorescence occurred. The increases at the two wavelengths were proportionate such that 340/365-nm ratios were unchanged. Thereafter, fluorescence at 365 nm decreased at a relatively constant rate. After about 16 min, fluorescence dropped abruptly. The disappearance of Fura-2 fluorescence coincided with the onset of propidium iodide staining (data not shown). These events signified hyperpermeability of the plasma membrane and onset of cell death.

Oxidation of Pyridine Nucleotides after Exposure to $HgCl_2$—Fluorescence of reduced pyridine nucleotides was measured in freshly isolated hepatocytes (Fig. 7). Before addition of $HgCl_2$, pyridine nucleotides were about 75% reduced. After 50 μM $HgCl_2$, fluorescence started to decrease within less than 30 s. After 2 min, pyridine nucleotides were maximally oxidized. The decrease of pyridine nucleotide fluorescence paralleled the increases of 340- and 365-nm fluorescence in Fura-2-loaded cells (Fig. 6).

Cell Viability in Freshly Isolated Hepatocyte Suspensions after Exposure to $HgCl_2$—After $HgCl_2$, free Ca^{2+} increased in high Ca^{2+} medium but not in low Ca^{2+} medium. However, loss of cell viability appeared to occur identically. To confirm the lack of effect of extracellular Ca^{2+} on cell killing, cell viability was measured in suspensions of hepatocytes using a propidium iodide cytotoxicity assay. Like trypan blue, propidium iodide is impermeable to viable cells, but binds to nuclei of nonviable cells. Since fluorescence of propidium iodide is enhanced following binding, this signal can be employed to monitor cell killing continuously in cell suspensions (14). Using the propidium iodide assay, $HgCl_2$ was observed to cause dose-dependent cell killing in suspensions of freshly isolated hepatocytes (see "Experimental Procedures"). Notably, the rate of cell killing was virtually identical in high and low Ca^{2+} media (Fig. 8).

Effect of $HgCl_2$ on Mitochondrial Membrane Potential—Changes of mitochondrial membrane potential in single cultured hepatocytes were monitored from rhodamine 123 fluorescence. After 50 μM $HgCl_2$, rhodamine 123 fluorescence began to increase to a maximal extent of about 50% after 2–3 min. Thereafter, total fluorescence decreased and a half-maximal decrease occurred after about 8 min (Fig. 9). These changes were virtually identical in high and low Ca^{2+} media (Fig. 9).

As illustrated for a representative experiment in Fig. 10, before addition of $HgCl_2$, rhodamine 123 was localized to mitochondria (Fig. 10*A*). By contrast, after 2.5 min of exposure to 50 μM $HgCl_2$, rhodamine 123 fluorescence was diffuse which indicated that dye had entered the cytosol from mitochondria. This abrupt redistribution of rhodamine 123 from mitochondria to cytosol was evidence of an early and rapid mitochondrial depolarization. Upon uptake into mitochondria, rhodamine 123 fluorescence is quenched by up to 75% (21). Thus, unquenching of rhodamine 123 as the fluorophore moves from the mitochondrial to the cytosolic compartment accounts for the rapid 50% increase of total cellular fluorescence observed after 2–3 min of $HgCl_2$ exposure (Fig. 9).

ATP Hydrolysis—In suspensions of hepatocytes, ATP declined sigmoidally after exposure to $HgCl_2$ (Fig. 11). After 1.5 min, ATP changed little, but between 2 and 5 min, ATP declined rapidly to less than 15% of initial values. The rate and extent of ATP hydrolysis was the same in high and low Ca^{2+} media. Comparing ATP with other parameters measured (Figs. 8, 9, and 11), ATP hydrolysis followed closely the depolarization of mitochondria but preceded bleb formation and cell death.

DISCUSSION

In this study we investigated the relationships of cytosolic free Ca^{2+}, mitochondrial membrane potential, pyridine nucleotide fluorescence, cell surface blebbing, and ATP content with respect to loss of cell viability after exposure of rat hepatocytes to $HgCl_2$. A series of cellular events occurred in the following order after 50 μM $HgCl_2$: oxidation of pyridine nucleotides (0.5–2 min), mitochondrial depolarization (2 min), ATP depletion (2–5 min), and bleb formation (4–5 min), increased cytosolic free Ca^{2+} in Ca^{2+}-containing buffer (6–7 min), and cell death (15–20 min). The timing and sequence

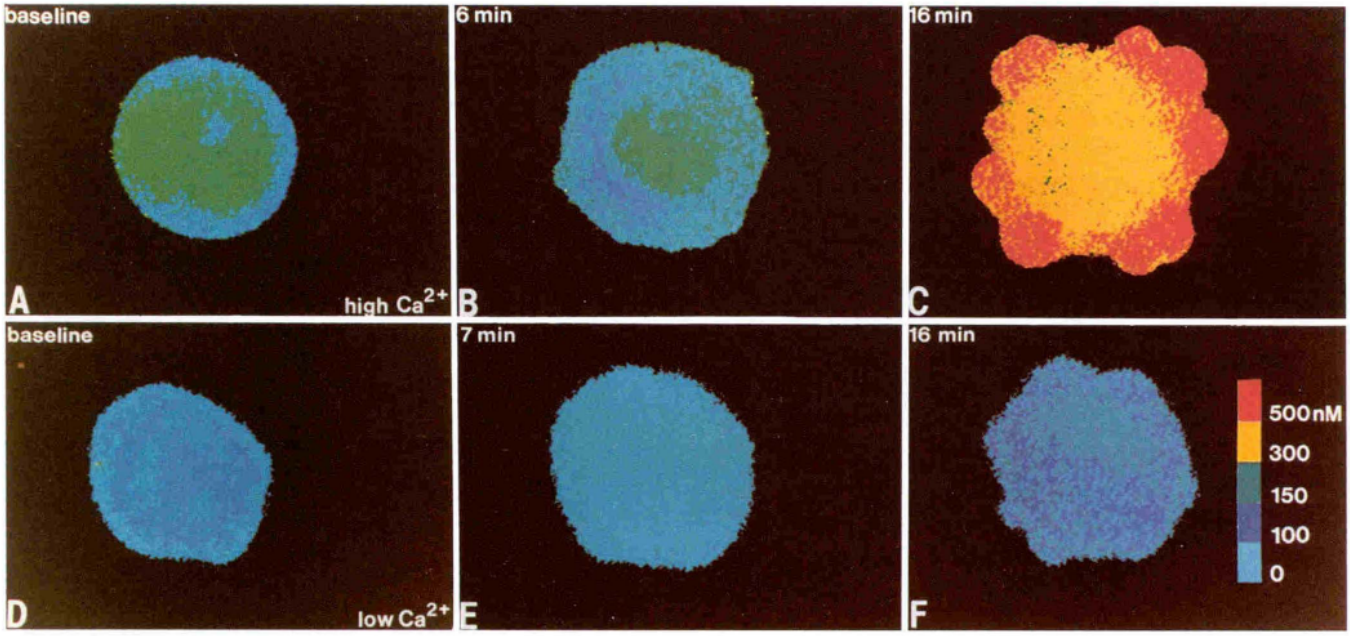

FIG. 5. **Spatial distribution of cytosolic free Ca^{2+} in single cultured hepatocytes after exposure to $HgCl_2$.** In Ca^{2+}-containing KHB buffer, basal free Ca^{2+} of a cultured hepatocyte averaged 175 nM as represented by *shades of blue* and *green* (*A*). After 6 min exposure to 50 μM $HgCl_2$, free Ca^{2+} averaged 160 nM (*B*), and blebbing was evident by bright field phase contrast microscopy, although not as well seen in the pseudo-color image. After 16 min free Ca^{2+} averaged 445 nM as represented by *orange* and *red* (*C*). Free Ca^{2+} was highest (*red*) in the large, well developed blebs. In low Ca^{2+} medium, basal free Ca^{2+} averaged 115 nM (*D*). After 7-min exposure to $HgCl_2$, free Ca^{2+} had actually decreased to 75 nM in this experiment (*E*), even though blebbing had begun. After 16 min, free Ca^{2+} still had not increased above base line (100 nM; *F*) despite the development of large surface blebs. In both experiments, cell death ensued after 16 min, and images could no longer be obtained.

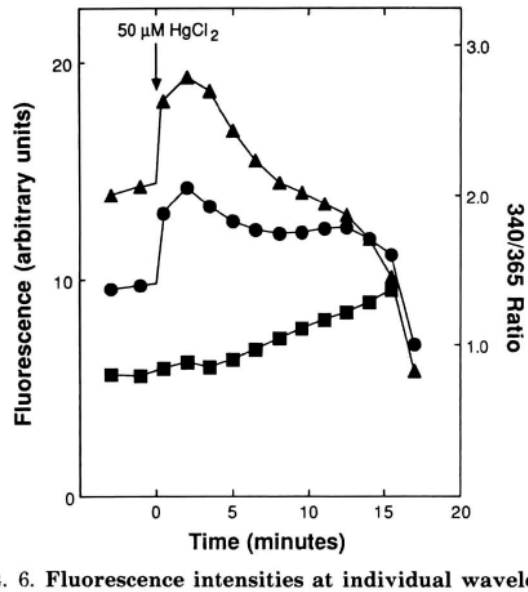

FIG. 6. **Fluorescence intensities at individual wavelengths in Fura-2-loaded hepatocytes after exposure to $HgCl_2$.** Cultured hepatocytes loaded with Fura-2 were incubated in high Ca^{2+} medium as described in Fig. 3. Fluorescence excited at 340 (●) and 365 nm and 340/365 ratio values (■) were measured using MDVM. $HgCl_2$ (50 μM) was added where indicated. The true isoemissive wavelength for Fura-2 through the microscope optics was between 360 and 365 nm, and fluorescence at 365 nm decreased slightly as Ca^{2+} increased. From a plot of 365 nm fluorescence *versus* free Ca^{2+} concentration, a corrected value for fluorescence at 365 nm was determined which corresponded to 365-nm fluorescence in 0 nM Ca^{2+} medium. This 365*-nm value (▲) was independent of Ca^{2+} and proportional only to Fura-2 concentration and fluorescence yield. One experiment representative of five.

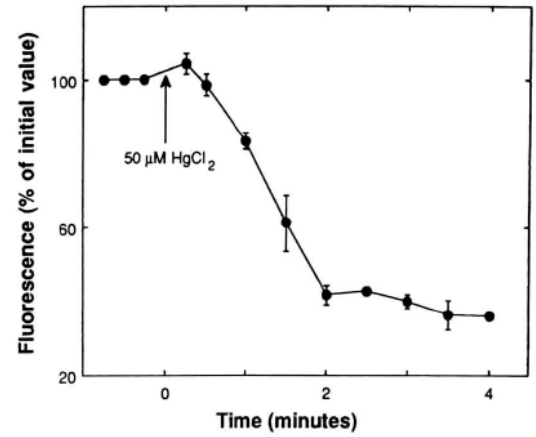

FIG. 7. **Pyridine nucleotide fluorescence in isolated hepatocytes after $HgCl_2$.** Freshly isolated hepatocytes (100,000 cells/ml) were incubated in KRH buffer. Pyridine nucleotide fluorescence was recorded as described under "Experimental Procedures" before and after addition of 50 μM $HgCl_2$ (*arrow*). In cells not treated with $HgCl_2$, fluorescence increased after 2.5 mM KCN (data not shown). Assuming 100% reduction after KCN and 0% reduction 2–4 min after $HgCl_2$, pyridine nucleotides were 75% reduced prior to addition of $HgCl_2$. Data represent means ± S.E. ($n = 4$).

of these events provided insight into the cellular and subcellular basis for toxic injury by $HgCl_2$.

Hg^{2+} binds with high affinity to protein and nonprotein thiols (10, 30) with consequent glutathione depletion and oxidative stress (31). In our model of $HgCl_2$ toxicity in rat hepatocytes, we observed a rapid oxidation of pyridine nucleotides beginning within 30 s and essentially complete after 2 min (Fig. 7). Mitochondrial depolarization closely followed pyridine nucleotide oxidation. We monitored mitochondrial

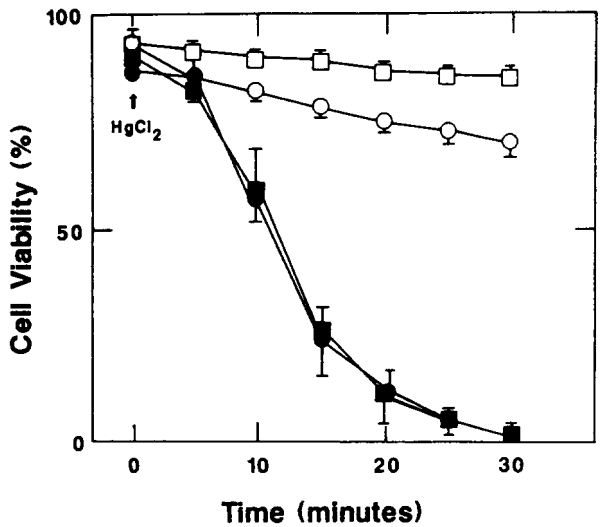

FIG. 8. **Viability of freshly isolated hepatocytes after $HgCl_2$ in low and high Ca^{2+} media.** Hepatocytes (100,000 cells/ml) were incubated 30 min at 37 °C in KRH buffer containing 2 mM $CaCl_2$ (high Ca^{2+}, □) or no added Ca^{2+} (low Ca^{2+}, ○). 50 μM $HgCl_2$ was added (*arrow*), and cell viability was assessed by propidium iodide fluorescence as described under "Experimental Procedures." Data represent means ± S.E. (n = 3). ●, low Ca^{2+} + $HgCl_2$; ■, high Ca^{2+} + $HgCl_2$.

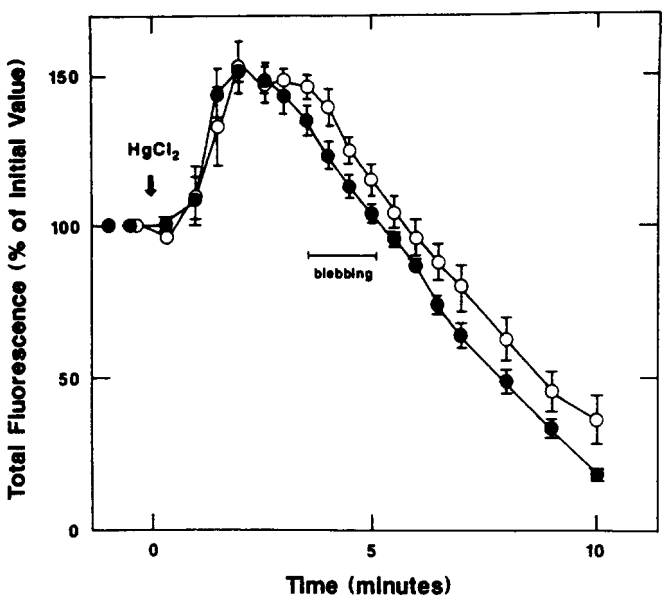

FIG. 9. **Rhodamine 123 fluorescence in cultured hepatocytes after $HgCl_2$ in low and high Ca^{2+} media.** Cultured hepatocytes were loaded with rhodamine 123 as described under "Experimental Procedures" and incubated in KHB containing high (●) or low (○) Ca^{2+}. Total cellular fluorescence of rhodamine 123 was measured using MDVM after addition of 50 μM $HgCl_2$ (*arrow*). Data represent means ± S.E. (n = 4).

membrane potential using rhodamine 123, a cationic fluorescent probe which accumulates electrophoretically into negatively charged compartments (21, 22). In normal cells, rhodamine 123 produced bright, punctate staining of mitochondria. After 50 μM $HgCl_2$, an abrupt redistribution of rhodamine 123 fluorescence from mitochondria to cytosol occurred after about 2 min (Fig. 10). This redistribution signified a collapse of the mitochondrial membrane potential. Thus, we observed *in situ* the phenomenon described in isolated mitochondria whereby pyridine nucleotide oxidation leads to mitochondrial depolarization and collapse of ion gradients (32).

Simultaneously with this abrupt redistribution of rhodamine 123 fluorescence, a 50% increase of total fluorescence of rhodamine 123 was observed (Fig. 9). When rhodamine 123 is taken up by isolated liver mitochondria, fluorescence is quenched by as much as 75% (21). Thus, the increase of total cellular fluorescence after $HgCl_2$ represented unquenching of fluorescence as rhodamine 123 moved from mitochondria to cytosol. Because total cellular fluorescence of rhodamine 123 decreased relatively slowly as dye leaked from the cells, imaging of rhodamine 123 redistribution from mitochondria to cytosol within individual cells was essential to capture dynamic changes of the mitochondrial membrane potential (Fig. 10).

Our observations of mitochondrial depolarization *in situ* confirm and extend previous reports of uncoupling and depolarization of mitochondria exposed to $HgCl_2$. Scott and Gamble (33) and Southard and co-workers (34) showed marked increases of permeability to K^+ and Mg^{2+} in isolated liver and heart mitochondria after 3–10 μM $HgCl_2$. Weinberg and co-workers (11) described uncoupling, respiratory inhibition, and increased atractyloside-insensitive adenine nucleotide translocation in isolated kidney mitochondria with as little as 1 μM $HgCl_2$. Similar changes were observed in kidney mitochondria isolated from $HgCl_2$-treated animals (8). Chavez and Holguin (10) documented pyridine nucleotide oxidation, Ca^{2+} release, and mitochondrial depolarization in isolated kidney mitochondria after 5 μM $HgCl_2$. The latter authors implicated Ca^{2+} recycling as a cause of depolarization. The present work documents pyridine nucleotide oxidation and mitochondrial depolarization *in situ* after $HgCl_2$. However, increases of cytosolic free Ca^{2+} coincident with mitochondrial depolarization were not observed even transiently during measurements made at 20-s intervals (Fig. 4). The explanation for the absence of a change of cytosolic free Ca^{2+} may simply be that the concentration of mitochondrial free Ca^{2+} was insufficient to perturb cytosolic Ca^{2+} upon equilibration of the mitochondrial matrix and the cytosol. Mitochondrial free Ca^{2+} has been estimated to be 500 nM or less in intact cells (35), and one recent report suggests that mitochondrial free Ca^{2+} is actually less than cytosolic (36). In any event, if mitochondrial Ca^{2+} recycling was occurring after $HgCl_2$, then it was occurring without a net change of cytosolic free Ca^{2+}.

ATP hydrolysis after $HgCl_2$ followed closely mitochondrial depolarization but preceded bleb formation, increased cytosolic Ca^{2+} (in high Ca^{2+} medium), and cell death (Fig. 11). Thus, ATP depletion appeared to be the consequence of uncoupling of oxidative phosphorylation. Interestingly, ATP depletion occurred at about the same rate and extent as when oxidative phosphorylation and glycolysis were inhibited with KCN and iodoacetate (chemical hypoxia) (14). Thus, the rapid decline of ATP after exposure to $HgCl_2$ suggests that glycolytic ATP synthesis was also inhibited, possibly by Hg^{2+} binding to reactive SH groups of glyceraldehyde-phosphate dehydrogenase. Inhibition of glycolysis would also explain why fructose, and effective glycolytic substrate which can prevent ATP depletion and cell death of anoxic hepatocytes (14, 37), did not delay or prevent cell killing caused by $HgCl_2$ (data not shown).

Jones and co-workers (38–40) have shown a generalized decrease of ion permeability of mitochondrial membranes in hepatocytes during anoxia. This permeability decrease is postulated to maintain near-normal mitochondrial membrane potentials and pH gradients during anoxic stress. With $HgCl_2$, collapse of the mitochondrial membrane potential and cell death were accelerated compared with chemical hypoxia under

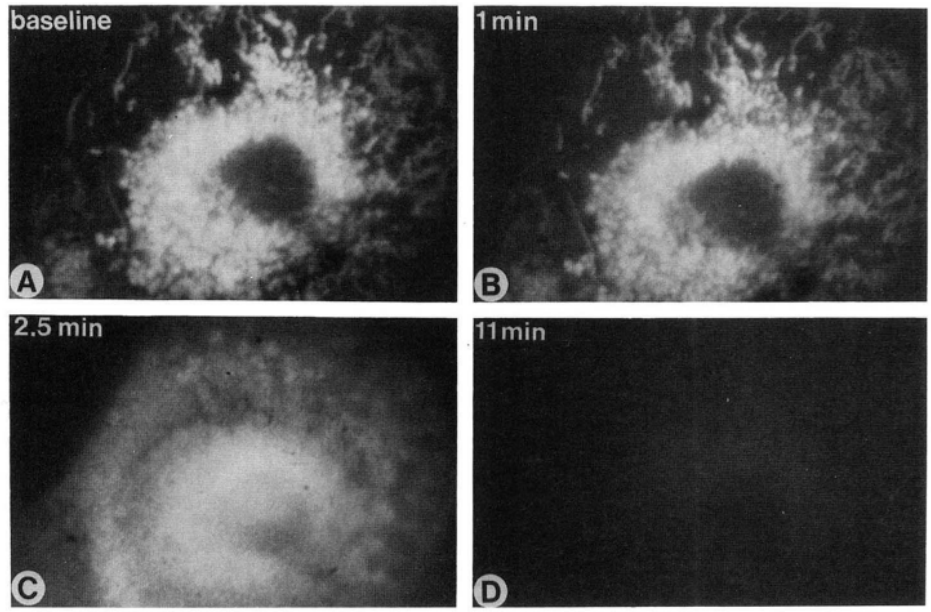

FIG. 10. **Intracellular distribution of rhodamine 123 in a cultured hepatocyte before and after $HgCl_2$.** A cultured hepatocyte was loaded with rhodamine 123 and incubated with $HgCl_2$ as described in Fig. 8. Before addition of $HgCl_2$, rhodamine 123 was localized to mitochondria (*A*). After 1 min of exposure to $HgCl_2$, fluorescence was still punctate and confined to mitochondria (*B*), but after 2.5 min, rhodamine 123 had redistributed from mitochondria into cytosol to make the cell diffusely fluorescent (*C*). After 11 min, most dye was lost from the cell (*D*).

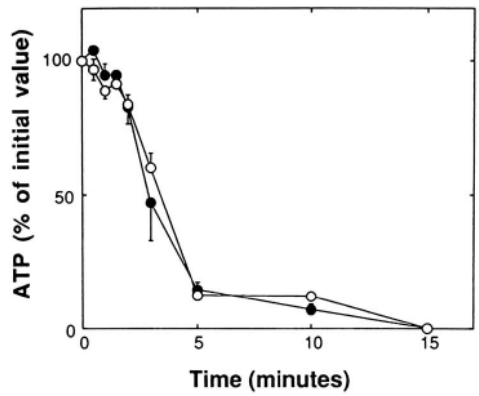

FIG. 11. **ATP depletion after exposure to $HgCl_2$ in low and high Ca^{2+} media.** Freshly isolated hepatocytes (100,000 cells/ml) were incubated in KRH containing low (○) or high (●) Ca^{2+} as described in Fig. 8. At various times after 50 μM $HgCl_2$, the cell suspensions were quenched, and ATP was determined as described under "Experimental Procedures."

nearly the same conditions. Thus, depolarization of the mitochondrial membrane potential may be an important factor, independent of ATP depletion, leading to the onset of cell death.

Cell surface blebbing is an early indication of hypoxic and toxic injury to hepatocytes (41–43). After $HgCl_2$, blebbing was evident after 4–5 min. Bleb formation followed ATP depletion, but preceded any increase of cytosolic free Ca^{2+}. Our earlier work had demonstrated similar blebbing following ATP depletion during anoxia and chemical hypoxia (5, 12). Thus, ATP depletion can account for blebbing during both reductive stress (anoxia, chemical hypoxia) and oxidative stress ($HgCl_2$ toxicity). High energy phosphate compounds are required for normal assembly and turnover of cytoskeletal elements. ATP depletion may disrupt these cytoskeletal structures to cause blebbing.

We employed Fura-2 to measure cytosolic free Ca^{2+} in single hepatocytes. The probe was introduced into cultured hepatocytes as its membrane-permeant acetoxymethyl ester. With this type of loading, intracellular esterases liberate Fura-2 free acid which is trapped inside the cells. For accurate measurement of cytosolic free Ca^{2+}, Fura-2 AM must be hydrolyzed completely and the free acid confined to cytosol. However, several reports indicate that this is not always the case. For example, Fura-2 AM may be incompletely hydrolyzed yielding fluorescent compounds which are insensitive to Ca^{2+} (27, 44). Furthermore, Fura-2 may localize to intracellular compartments other than cytosol (*e.g.* mitochondria, lysosomes, secretory granules, and endoplasmic reticulum, Refs. 27 and 44–49). In view of these concerns, we evaluated the degree of hydrolysis and subcellular localization of the dye. In one set of experiments, we released Fura-2 from freshly isolated hepatocytes using digitonin and Triton X-100. Digitonin (100 μM) released 93% of the fluorescence released by Triton X-100 (0.1%) (Table I). Since digitonin permeabilizes plasma membranes but not mitochondrial membranes, whereas Triton X-100 solubilizes all cellular membranes, we conclude that more than 90% of Fura-2 was in a nonmitochondrial compartment.

Compared with pure Fura-2 free acid, subtle differences were observed for Fura-2 fluorescence released from digitonin-treated cells. The 340/380-nm ratio in high Ca^{2+} medium was lower than that for pure free acid, possibly because of products of incomplete hydrolysis or other metabolism (27) (Table II). By contrast, the 340/365-nm ratio was unchanged. Hence, we employed 340/365-nm fluorescence ratios to measure free Ca^{2+}. This approach had the additional advantage of allowing us to monitor cellular dye content at 365 nm.

We further localized Fura-2 in loaded hepatocytes using MDVM. Employing specific markers for mitochondria (Fig. 1) and lysosomes (Fig. 2), we developed a procedure for sequentially releasing Fura-2 from cytosol (with 20 μM digitonin), lysosomes (100 μM digitonin), and mitochondria (0.1% Triton X-100). The results indicated that 83% of Fura-2 AM was cytosolic, 11% in lysosomes (and other endomembrane compartments), and 6% in mitochondria (Table I). The predominantly cytosolic localization of Fura-2 justified its use to monitor cytosolic free Ca^{2+} during $HgCl_2$ toxicity.

$HgCl_2$ (50 μM) caused a 3–4-fold increase of free cytosolic Ca^{2+} beginning after 6–7 min in high Ca^{2+} medium (Fig. 3). In low Ca^{2+} medium, free Ca^{2+} did not change. Thus, the source of increased free Ca^{2+} was extracellular. In high Ca^{2+} medium, spatial gradients of Ca^{2+} also developed within cells, and blebs became hot spots of free Ca^{2+} (>600 nM) (Fig. 5).

This observation suggests that Ca^{2+} entry was accelerated through the plasma membranes of blebs. Significantly, rates of cell killing and the onset of bleb formation were virtually identical in both Ca^{2+}-containing and Ca^{2+}-free buffers (Fig. 5). Thus, a rise of cytosolic free Ca^{2+} was not a necessary stimulus for bleb formation or the final common pathway to cell death.

Nonspecific changes of Fura-2 fluorescence were also observed after $HgCl_2$. After 1–2 min, fluorescence of Fura-2 increased by about 40% at both excitation wavelengths (Fig. 6). This abrupt increase was not due to an increase of free cytosolic Ca^{2+}, since 340/365 nm ratios were unaffected. As the amount of Fura-2 in the cell could not have increased, we conclude that some early event after $HgCl_2$ addition was producing an unquenching of Fura-2 fluorescence. However, this was not due to direct interaction of $HgCl_2$ with Fura-2. Notably, oxidation of pyridine nucleotides paralleled the increases of fluorescence (Fig. 7). NADH and NADPH absorb strongly with a broad maximum at 340 nm, whereas NAD and NADP do not. Thus, increases of Fura-2 fluorescence after $HgCl_2$ may simply reflect the reversal of colorimetric quenching by NAD(P)H and possibly other compounds. In any event, ratio imaging appropriately corrected for this artifact, whatever its source.

After the initial increase, total fluorescence at 365 nm decreased steadily for about 15 min at which point cells began to lose fluorescence very rapidly as viability was lost. In hepatocytes not treated with $HgCl_2$, Fura-2 fluorescence did not decrease after more than 30 min of incubation indicating that neither photobleaching nor dye leakage occurred in control cells. Although we cannot distinguish between quenching and dye leakage in this context, the data do suggest a leakage of Fura-2 after treatment with $HgCl_2$ as described by Smith and co-workers (9) for kidney tubule cells. Despite the loss of Fura-2, cells continued to exclude propidium iodide up to the point of death. The latter observation suggests that loss of Fura-2 might occur by a relatively specific pathway. However, probenecid (10 μM and 1 mM), an inhibitor of organic anion transport (50), did not diminish leakage of Fura-2 after $HgCl_2$ treatment (data not shown).

In contrast to our findings, Smith and co-workers (9) recently reported a 10–12-fold increase of free cytosolic Ca^{2+} after 1 min of exposure of rabbit renal tubular cells to $HgCl_2$ followed by a recovery to a 2-fold steady state increase after 3 min. Subsequently, a slower secondary increase of free Ca^{2+} was described which was dependent on extracellular Ca^{2+}. These measurements were made employing Fura-2 fluorescence excited at 340 nm without ratioing. Our data showing large Ca^{2+}-independent changes of Fura-2 fluorescence after $HgCl_2$ suggest that the early fluorescence changes observed by Smith *et al.* (9) may not have been due to changes in free Ca^{2+} but rather to an unquenching phenomenon. Moreover, our data showing leakage of Fura-2 from dead and injured cells suggest that Fura-2 leakage into Ca^{2+}-containing extracellular medium may have accounted in large part for the later increase of Fura-2 fluorescence observed by Smith and co-workers (9).

The calcium hypothesis of cell killing has been a provocative proposal which has stimulated much new experimental work. However, our data in hepatocytes indicates that an increase of free Ca^{2+} is not in the causal chain of events leading to cell death from toxic and hypoxic injury. During chemical hypoxia, a model of ATP depletion by metabolic inhibition of respiration and glycolysis, cytosolic free Ca^{2+} did not increase as expected prior to bleb formation or the onset of cell death (5). In more recent studies, a transient increase of free Ca^{2+} was documented just at the onset of cell death as propidium iodide began to enter cells and trapped dyes such as Fura-2 began to exit (6). This transient increase was not observed in Ca^{2+}-free medium, although the rate of cell killing was identical. In the present study, we observed a sustained increase of free Ca^{2+} after $HgCl_2$ which began well prior to cell killing. Again, this increase did not occur in Ca^{2+}-free medium even though the rate of killing was the same. These data indicate clearly that an increase of free Ca^{2+} was not required for bleb formation and cell death. Furthermore, an elevation of free Ca^{2+}, even when it occurred, did not accelerate the onset of cell death.

In conclusion, our results indicate that following oxidative stress with $HgCl_2$, mitochondria depolarize and presumably uncouple leading to ATP depletion, bleb formation, and ultimately cell death. This bioenergetic lesion seems sufficient to explain lethal injury from $HgCl_2$. However, multisite actions of $HgCl_2$, such as leakiness of the plasma membrane and resulting loss of ion gradients, may also contribute to lethal cell injury (15). For example, ATP hydrolysis to AMP releases two hydrogen ions. During chemical hypoxia, the resulting intracellular acidosis protects against the onset of cell death during chemical hypoxia (14, 51). Membrane leakiness produced by $HgCl_2$ may dissipate such a pH gradient causing cytosolic pH to remain at neutrality and cell killing to be accelerated. Multiparameter digitized video microscopy should continue to be useful in elucidating the role of intracellular pH and other factors in toxic cell injury.

REFERENCES

1. Schanne, F. A. X., Kane, A. B., Young, E. E., and Farber, J. L. (1979) *Science* **206,** 700–702
2. Nicotera, P., Hartzell, P., Baldi, C., Svensson, S.-Å., Bellomo, G., and Orrenius, S. (1986) *J. Biol. Chem.* **261,** 14628–14635
3. Chien, K. R., Abrams, J., Serroni, A., Martin, J. T., and Farber, J. L. (1978) *J. Biol. Chem.* **253,** 4809–4817
4. McConkey, D. J., Hartzell, P., Nicotera, P., Wyllie, A. H., and Orrenius, S. (1988) *Toxicol. Lett.* **42,** 123–130
5. Lemasters, J. J., DiGuiseppi, J., Nieminen, A.-L., and Herman, B. (1987) *Nature* **325,** 78–81
6. Nieminen, A.-L., Gores, G. J., Wray, B. E., Tanaka, Y., Herman, B., and Lemasters, J. J. (1988) *Cell Calcium* **9,** 237–246
7. Weinberg, J. M., Harding, P. G., and Humes, H. D. (1983) *Exp. Mol. Pathol.* **39,** 43–60
8. Weinberg, J. M., Harding, P. G., and Humes, H. D. (1982) *J. Biol. Chem.* **257,** 68–74
9. Smith, M. W., Ambudkar, I. S., Phelps, P. C., Regec, A. L., and Trump, B. F. (1987) *Biochim. Biophys. Acta* **931,** 130–142
10. Chavez, E., and Holguín, J. A. (1988) *J. Biol. Chem.* **263,** 3582–3587
11. Weinberg, J. M., Harding, P. G., and Humes, H. D. (1982) *J. Biol. Chem.* **257,** 60–67
12. Herman, B., Nieminen, A.-L., Gores, G. J., and Lemasters, J. J. (1988) *FASEB J.* **2,** 146–151
13. Strain, A. J., McGowan, J. A., and Bucher, N. L. R. (1982) *In Vitro* **18,** 108–116
14. Gores, G. J., Nieminen, A.-L., Dawson, T. L., Herman, B., and Lemasters, J. J. (1988) *Am. J. Physiol.* **255,** C315–C322
15. Ballatori, N., Shi, C., and Boyer, J. L. (1988) *Toxicol. Appl. Pharmacol.* **95,** 279–291
16. Schweinsberg, P. D., and Loo, T. L. (1980) *J. Chromatogr.* **181,** 103–107
17. Jones, D. P. (1981) *J. Chromatogr.* **225,** 446–449
18. Kao, J. P. Y., Harootunian, A. T., and Tsien, R. Y. (1989) *J. Biol. Chem.* **264,** 8179–8184
19. DiGuiseppi, J., Inman, R., Ishihara, A., Jacobson, K., and Herman, B. (1985) *BioTechniques* **3,** 394–403
20. Grynkiewicz, G., Poenie, M., and Tsien, R. Y. (1985) *J. Biol. Chem.* **260,** 3440–3450
21. Emaus, R. K., Grunwald, R., and Lemasters, J. J. (1986) *Biochim. Biophys. Acta* **850,** 436–448
22. Johnson, L. V., Walsh, M. L., Bockus, B. J., and Chen, L. B. (1981) *J. Cell Biol.* **88,** 526–535

23. Krishan, A. (1975) *J. Cell Biol.* **66,** 188–193
24. Ohkuma, S., and Poole, B. (1978) *Proc. Natl. Acad. Sci. U. S. A.* **75,** 3327–3331
25. Gores, G. J., Flarsheim, C. E., Dawson, T. L., Nieminen, A.-L., Herman, B., and Lemasters, J. J. (1989) *Am. J. Physiol.* **257,** C347–C354
26. Loud, A. V. (1968) *J. Cell Biol.* **37,** 27–46
27. Scanlon, M., Williams, D. A., and Fay, F. S. (1987) *J. Biol. Chem.* **262,** 6308–6312
28. Fiskum, G., Craig, S. W., Decker, G. L., and Lehninger, A. L. (1980) *Proc. Natl. Acad. Sci. U. S. A.* **77,** 3430–3434
29. Meredith, M. J., and Reed, D. J. (1982) *J. Biol. Chem.* **257,** 3747–3753
30. Baggett, J. M., and Berndt, W. O. (1986) *Toxicol. Appl. Pharmacol.* **83,** 556–562
31. Gstraunthaler, G., Pfaller, W., and Kotanko, P. (1983) *Biochem. Pharmacol.* **32,** 2969–2972
32. Beatrice, M. C., Palmer, J. W., and Pfeiffer, D. R. (1980) *J. Biol. Chem.* **255,** 8663–8671
33. Scott, R. L., and Gamble, J. L., Jr. (1961) *J. Biol. Chem.* **236,** 570–573
34. Southard, J., Nitisewojo, P., and Green, D. E. (1974) *Fed. Proc.* **33,** 2147–2153
35. McCormack, J. G., and Denton, R. M. (1988) in *Integration of Mitochondrial Function* (Lemasters, J. J., Hackenbrock, C. R., Thurman, R. G., and Westerhoff, H. V., eds) pp. 487–496, Plenum Publishing Corp., New York
36. Moreno-Sanchez, R., and Hansford, R. G. (1988) *Biochem. J.* **256,** 403–412
37. Anundi, I., King, J., Owen, D. A., Schneider, H., Lemasters, J. J., and Thurman, R. G. (1987) *Am. J. Physiol.* **253,** G390–G396
38. Andersson, B. S., Aw, T. Y., and Jones, D. P. (1987) *Am. J. Physiol.* **252,** C349–C355
39. Aw, T. Y., Andersson, B. S., and Jones, D. P. (1987) *Am. J. Physiol.* **252,** C356–C361
40. Aw, T. Y., Andersson, B. S., and Jones, D. P. (1987) *Am. J. Physiol.* **252,** C362–C368
41. Lemasters, J. J., Ji, S., and Thurman, R. G. (1981) *Science* **213,** 661–663
42. Jewell, S. A., Bellomo, G., Thor, H., Smith, M. T., and Orrenius, S. (1982) *Science* **217,** 1257–1259
43. Lemasters, J. J., Stemkowski, C. J., Ji, S., and Thurman, R. G. (1983) *J. Cell Biol.* **97,** 778–786
44. Oakes, S. G., Martin, W. J., II, Lisek, C. A., and Powis, G. (1988) *Anal. Biochem.* **169,** 159–166
45. Steinberg, S. F., Bilezikian, J. P., and Al-Awqati, Q. (1987) *Am. J. Physiol.* **253,** C744–C747
46. Malgaroli, A., Milani, D., Meldolesi, J., and Pozzan, T. (1987) *J. Cell Biol.* **105,** 2145–2155
47. Almers, W., and Neher, E. (1985) *FEBS Lett.* **192,** 13–18
48. Highsmith, S., Bloebaum, P., and Snowdowne, K. W. (1986) *Biochem. Biophys. Res. Commun.* **138,** 1153–1162
49. Roe, M. W., Lemasters, J. J., and Herman, B. (1987) *Fed. Proc.* **46,** a2277
50. Steinberg, T. H., Newman, A. S., Swanson, J. A., and Silverstein, S. C. (1987) *J. Cell Biol.* **105,** 2695–2702
51. Gores, G. J., Nieminen, A.-L., Wray, B. E., Herman, B., and Lemasters, J. J. (1989) *J. Clin. Invest.* **83,** 386–396
52. Nieminen, A.-L., Gores, G. J., Herman, B., and Lemasters, J. J. (1988) *FASEB J.* **2,** A825